Highlights

Solid solution strengthening in medium- to high-entropy alloys

J. Freudenberger, F. Thiel, D. Utt, K. Albe, A. Kauffmann, S. Seils, M. Heilmaier

- Au-Cu-Ni-Pd-Pt alloys with deliberately adjusted composition, in particular $(ABCD)_{100-x}E_x$ alloy series, are single phase
- Within Au-Cu-Ni-Pd-Pt alloys, the effect of solid solution strengthening can be solely investigated as other strengthening mechanisms can be minimised or eliminated
- The contribution of solid solution strengthening of some $(ABCD)_{100-x}E_x$ alloy series is in agreement with established models of solid solution strengthening others strongly deviate.
- The mechanical properties of the $(AuCuPdPt)_{100-x}Ni_x$ series are in agreement with the theory of Varvenne et al.

Solid solution strengthening in medium- to high-entropy alloys

J. Freudenberger[a,b,*], F. Thiel, D. Utt[c], K. Albe[c], A. Kauffmann[d], S. Seils[d,e], M. Heilmaier[d]

[a] *Leibniz-IFW Dresden, Helmholtzstraße 20, D-01069 Dresden, Germany*
[b] *TU Bergakademie Freiberg, Institute of Materials Science, Gustav-Zeuner-Straße 5, D-09599 Freiberg, Germany*
[c] *TU Darmstadt, Institut für Materialwissenschaft, Otto-Berndt-Str. 3, D-64287 Darmstadt, Germany*
[d] *Karlsruhe Institute of Technology (KIT), Institute for Applied Materials (IAM-WK), Engelbert-Arnold-Straße 4, D-76131 Karlsruhe, Germany*
[e] *Karlsruhe Institute of Technology (KIT), Karlsruhe Nano Micro Facility (KNMF), Hermann-von-Helmholtz-Platz 1, D-76344 Eggenstein-Leopoldshafen, Germany*

Abstract

A fundamental understanding of the strength of multi-component alloys relies on well-defined experiments accompanied by accurate modelling. Whilst much work has been done so far for equi-atomic alloys, little has been done to investigate the effect of solid solution strengthening for alloys with deliberately adjusted, non-equimolar composition that are varied in certain concentration steps, including particularly continuous changes between equimolar subsets of alloy systems. This systematic approach is a key tool to verify or falsify current theories for solid solution strengthening for highly concentrated alloys. Series of alloys where a fifth element is alloyed to an equi-atomic four component alloy were prepared from Au, Cu, Ni, Pd and Pt, respectively. All investigated alloys form a single-phase solid solution, which is proven on a wide range of length scale by means of XRD, SEM and APT measurements. The mechanical properties of the series are compared to the predicted yield stresses calculated upon the model of Varvenne et al. [1]. The present results highlight coincident and discrepant results between experiment and model.

Keywords: high-entropy alloy, precious metals, solid solution strengthening, mechanical properties, microstructure

1. Introduction

Single-phase multicomponent alloys without principle elements, also denoted as high-entropy alloys (HEAs), exhibit enhanced mechanical properties compared to dilute single-phased alloys [2, 3]. This was deduced from severe solid solution strengthening [4–6]. However, classic theories for solid solution strengthening, i.e. Labusch-type weak-pinning model, were made for solutions with solvents of at most 10 at.% in a single component matrix [7]. These theories are not valid for HEAs, where solutes and solvents cannot be clearly identified. Thus, a key issue of current research in the field of HEAs is the development of theoretical models for solid solution strengthening in highly concentrated alloys and in particular of alloys without principal element.

*Corresponding author.
Email address: j.freudenberger@ifw-dresden.de (J. Freudenberger)

With the help of theory, the strength of highly concentrated alloys shall be described and possibly predicted. However, this is challenging for three main reasons. (i) Commonly, multi-component alloys contain several phases. In consequence, the whole realm of strengthening mechanisms has to be considered when modelling the yield stress, including also phase boundary hardening arising from precipitates and/or dispersoids. The task of analysing solid solution strengthening while considering all active strengthening mechanisms eases when the number of other mechanisms is reduced, or their contribution to the total strength is minimised. In order to precisely evaluate solid solution strengthening of an alloy, it should be single phase and the microstructure should have low densities of grain boundaries and dislocations. (ii) It is essential to be capable of realising variations in the composition without abandoning the single phase or changing the microstructure. However, this is not necessarily the case due to often observed limited solubilities. (iii) The analysis of the interaction forces, based on parelastic (variation of the lattice parameter), dielastic (variations of the shear modulus) and chemical (variations of the stacking fault energy) interactions, becomes more complex in multi-component alloys [8].

The most promising theory of solid solution strengthening in fcc multicomponent alloys was developed by C. Varvenne et al. [1, 4, 9] as an extension of the Labusch-type weak-pinning model [7]. The key problem for this extension arises from the indistinguishability of matrix and solute elements, i.e. there is no basis element in HEAs, where the different components occur in similar concentration. Thus, the differentiation of matrix and solute elements, representing the classification of conventional alloys does not work for HEAs. Consequently, this also holds for the classic theories which were made for conventional alloys with concentrations of solutes well below 10%. For this purpose, Varvenne et al. [4] define an effective averaged matrix, representing the mean concentration-weighted properties of the alloy components. The strengthening effect arise from local concentration fluctuations leading to attracting and repelling forces on the dislocation line and, thus, a wavy equilibrium dislocation line shape. At the expense of dislocation line energy, sections of the dislocation line would bow out into regions with lower potential energy due to an ideal local elemental pairing. Moving the dislocation out of this potential energy minimum, a higher shear stress is necessarily causing an increased yield stress of the HEA [4].

The model clearly identified which material parameters play a major role for strengthening, i.e. (i) the strength does not directly depend on the number of elements in the alloy, (ii) the shear modulus G and the concentration-weighted mean-square misfit volume quantity ΔV are the key parameters for the determination of the strength and (iii) the stacking fault energy has little influence on the strength [1, 4]. On the other hand, this model also bears some significant drawbacks as e.g. it assumes a random distribution of the components on the lattice sites, which is presumably not the case. Thus, possible influences of short range order (SRO), nano-sized precipitates or phase decomposition could reveal misleading experimental results. However, the contribution of SRO to the mechanical strength is part of controversial discussions [10–14]. An extension of Varvenne's model considering these issues was incorporated by Antillon et al. [15].

The validity of Varvenne's model was proven for several HEA systems, i.e. Co-Cr-Fe-Mn-Ni [4, 16–19], $CoCrFeNiAl_x$ [20] and various noble metal HEAs [9, 21] and is in reasonable accordance to experimental data. However, an in-depth analysis of solid solution strengthening in these alloys is often limited to equiatomic compositions due to the occurrence of secondary phases or structural changes, including SRO. Consequently, the compositional space in the vicinity of the HEA is disregarded so far.

As mentioned before, regarding the experimental validation of these models, solid solutions are required that also allow variations of the composition in a large range, ideally in the whole compositional space. This will allow the evaluation of models for solid solution strengthening by a more detailed investigation in dependence on compositional changes which is thus not limited to a sole composition, only. Therefore, the investigation of high-entropy alloys with deliberately adjusted composition is a key tool to verify or falsify current theories for solid solution strengthening for highly concentrated alloys. The Au-Cu-Ni-Pd-Pt alloys comply with the mentioned requirements and are unique in the sense, that they are single phase and the homogeneous solid solutions presumably span the entire range of chemical compositions including the elements, binary, ternary, quaternary and in particular the quinary alloys [22, 23]. Consequently, a compositional dependent study of the mechanical properties of these alloys will allow for the validation of solid solution strengthening theories, which gives this system benchmark character with regard to other single-phase high entropy alloys.

The present study is focussed on the investigation of the mechanical response of single-phase multi-component alloys of the precious metal-based HEA system Au-Cu-Ni-Pd-Pt. The composition of the investigated alloys were adjusted so that series from four-component medium-entropy alloys to the HEA AuCuNiPdPt were obtained, i.e. $(\mathrm{ABCD})_{100-x}\mathrm{E}_x$, where A,B,C,D and E represent one of the given elements. In what follows, these series are denoted as 4+x series. Within this wide concentration range of $0 \leq x \leq 20$ at.%, the mechanical properties are compared to the theoretically assessed contributions of solid solution strengthening to the yield stress calculated by the model of Varvenne et al. [1, 4].

2. Materials and Methods

2.1. Processing

For investigating the concentration-dependent properties, $(\mathrm{ABCD})_{100-x}\mathrm{E}_x$ alloy series were prepared from pure elements. The purities and suppliers are as follows. Au: 4N, Allgemeine Gold- und Silberscheideanstalt AG (AGOSI); Cu: 5N5, VEB Spurenmetalle Freiberg/Sa.; Ni: 4N, Alfa Aesar; Pd: 3N5, AGOSI; Pt: 4N, AGOSI. Initially, four-component equi-molar master alloys were synthesised by arc melting (Edmund Buehler GmbH) in an Ar atmosphere on a water-cooled Cu mould. In order to ensure a uniform elemental distribution, alloys were melted four times with turning the ingot over in between the melting steps. Afterwards, rod-shaped samples were obtained by centrifugal casting (Linn High Therm GmbH) into a copper mould of 8.9 mm in diameter and 150 mm in length. After a homogenisation heat treatment the samples were sectioned for further processing. Series of $(\mathrm{ABCD})_{100-x}\mathrm{E}_x$ alloys (hereafter also denoted as 4+x) were prepared from sections of the four-component master alloys and an addition of the fifth element of $x = 0$, 1, 3, 5, 7, 10, 15, 20 at.%, respectively. These samples were also arc-melted four times and the ingots were turned over in between the melting steps. Finally, the samples were suction cast into a water-cooled Cu mould with a diameter and length of 4 mm and 75 mm, respectively.

The as-cast alloys were homogenised at 1000 °C to 1200 °C depending on the composition for 20 h with subsequent water-quenching. The proper homogenisation temperature T_h of any individual alloy has been determined previously by differential scanning calorimetry and set to be at least $T_\mathrm{h} \simeq 0.9\,T_\mathrm{m}$, with T_m being the solidus temperature of the alloy. This high temperature

is required to avoid decomposition which might occur at low temperatures. Annealing was performed in sealed fused silica ampoules under protective Ar atmosphere, which were destroyed after annealing to allow for rapid water-quenching.

The homogenised samples were cold worked by rotary swaging (UR2-4, Heinrich Müller Maschinenfabrik, Pforzheim) at room temperature with an area reduction per step of approximately $\varphi = 0.2$ and a total logarithmic degree of deformation of $\varphi_{\mathrm{tot}} = 0.6$ ($\varphi = \ln(A_i/A_f)$, where A_i and A_f are the initial and final cross sectional area, respectively). Afterwards, the samples were heat treated for 1 h at the same temperature and circumstances as mentioned before in order to obtain a fully recrystallised microstructure.

2.2. Characterisation methods

For microstructural analysis and microhardness tests, the samples were embedded in epoxy resin and prepared by a conventional metallographic procedure, which includes grinding on abrasive SiC paper up to a grid size of P4000, polishing on MD-Mol and MD-Nap cloths (Struers) using diamond suspension (MetaDi Supreme suspension, Buehler) with a net particle size of 3 µm, 1 µm, and 0.25 µm, respectively. To remove the residual surface-near deformation layer, etching with diluted aqua regia (25 % H_2O) was applied for 30 s.

Structural characterisation by X-ray diffraction (XRD) was done on bulk samples (thickness $\leq$ 30 µm) utilising a STOE STADI_P diffractometer with $MoK_{\alpha 1}$ radiation (0.709 32 nm) in Debye-Scherrer geometry equipped with a position sensitive detector (PSD) Dectris Mythen 1K and a curved Ge(111)-monochromator (step size $\Delta\theta = 0.01\,^\circ$).

Microstructural characterisation was carried out by scanning electron microscopy (SEM) utilising an FEI Helios 600i operating at 10 kV and 1.4 nA with back-scattered electron contrast. The determination of mean grain size was done by the linear intercept method using Imagic IMS software.

Microhardness measurements were performed utilising a Shimadzu HMV-2 hardness tester at a load of 1.98 N. For sound statistics, the microhardness was evaluated from at least 15 indentations. In order to rule out the effect of dislocation pile-up strengthening, the indentations were placed on the surface away from grain boundaries. Compressive tests were performed at RT with a constant crosshead movement corresponding to an initial engineering strain rate of $\dot{\varepsilon} = 1 \cdot 10^{-3}\,\mathrm{s}^{-1}$ using an electro-mechanical Instron 5869 testing machine. For this purpose, samples with a diameter of $d_0 = 2.8$ mm and a height of $h_0 \lesssim 6$ mm were used ($1.5 \lesssim h_0/d_0 \lesssim 2$). The tests were stopped when the aspect ratio approached h/d = 1. The strain was measured with the help of a laser extensometer in between the edges of the plungers.

Atom probe tomography (APT) was utilised to evaluate uniform element distribution after recrystallisation. At least three sample tips were entirely prepared from grain volume with a FIB FEI Strata utilising the standard lift-out method on a microtip coupon [24, 25]. The analyses were performed with a local electrode atom probe (LEAP 4000X HR, Cameca) at a temperature of about 50 K at a pulse frequency of 125 kHz and a pulse energy of 50 pJ. For the evaluation of the APT results, the Cameca software IVAS 3.6.14 was used.

2.3. Model-based determination of solid solution strengthening

Modelling of solid solution strengthening in fcc alloys was performed by using the reduced theory including only elastic contributions derived by Varvenne et al. [4]. Eqs. 1-3 give the

critical shear stress for dislocation glide $\tau_{\mathrm{c,ss}}$ as function of temperature T and strain rate $\dot{\varepsilon}$:

$$\Delta\tau_{\mathrm{c,ss}}\left(T,\dot{\varepsilon}\right)=\tau_0\left[1-\left(\frac{k_{\mathrm{B}}T}{\Delta E_{\mathrm{b}}}\ln\frac{\dot{\varepsilon}_0}{\dot{\varepsilon}}\right)^{\frac{2}{3}}\right] \tag{1}$$

$$\tau_0=0.01785\alpha^{-\frac{1}{3}}\bar{G}\left(\frac{1+\bar{\nu}}{1-\bar{\nu}}\right)^{\frac{4}{3}}\left[\frac{\sum_i x_i\Delta V_i^2}{b^6}\right]^{\frac{2}{3}} \tag{2}$$

$$\Delta E_{\mathrm{b}}=1.5618\alpha^{\frac{1}{3}}\bar{G}b^3\left(\frac{1+\bar{\nu}}{1-\bar{\nu}}\right)^{\frac{2}{3}}\left[\frac{\sum_i x_i\Delta V_i^2}{b^6}\right]^{\frac{1}{3}} \tag{3}$$

where $\bar{G}$ and $\bar{\nu}$ are the mean composition-weight shear modulus and Poisson's ratio of the alloys, respectively. x_i is the concentration of element i. ΔV_i is the misfit volume, b is the length of the Burgers vector and k_{B} is the Boltzmann constant. Consistent to Varvenne and Curtin [9], we chose the following parameters: $T=300\,\mathrm{K}$, $\alpha=0.123$, $\dot{\varepsilon}=10^{-4}\,\mathrm{s}^{-1}$, and $\dot{\varepsilon}_0=10^4\,\mathrm{s}^{-1}$. The line tension parameter $\alpha=0.123$ was obtained from atomistically measured edge dislocation line tension in the embedded atom method for an effective FeNiCr matrix and is close to the coefficient for elemental Al [4, 26]. This value is not available for the Au-Cu-Ni-Pd-Pt-system. For a rough estimate, we used this value for the current analysis. This parameter will not change the trends observed and, therefore, will not affect the following discussion regarding the discrepancy between model and experiment. C. Varvenne et al. stated [4] that $\dot{\epsilon}$ will always appear within a logarithm, values within one order of magnitude of this estimate make little quantitative difference in final predictions of the yield stress. The contribution of solid solution strengthening to the yield stress, $\Delta\sigma_{\mathrm{c,ss}}$, was calculated upon $\Delta\tau_{\mathrm{c,ss}}$ using a Taylor factor of 3.06 assuming random orientation of the grains within the fcc material.

As many of the input parameters which are required for modelling are not known for the Au-Cu-Ni-Pd-Pt alloys, we follow the approach taken in Ref. [9] and use Vegard's rule of mixture [27] based on established literature data from Ref. [28], with $\bar{G}=\sum_i x_i G_i$ and $\bar{\nu}=\bar{E}/2\bar{G}-1$, where the Young's moduli of the alloys are determined upon $\bar{E}=\sum_i x_i E_i$. Furthermore, the mean atomic volumes of the alloys are calculated upon $\bar{V}=\frac{1}{4}\left(\sum_i x_i a_i\right)^3$, which is further used to calculate the misfit volume $\Delta V_i=V_i-\bar{V}$. The used input parameters, i.e. a_i, G_i and E_i are provided in Tab. 1.

The key misfit quantity of the model is $\sum_i x_i\Delta V_i^2$. According to Varvenne et al. [9], this parameter is closely related to the misfit parameter δ that is widely used to characterise multi-component alloys. When the elements in an alloy form a solid solution, which is the case for the Au-Cu-Ni-Pd-Pt alloys, this parameter δ is written as follows:

$$\delta=\sqrt{2\sum_i x_i\Delta V_i^2/9b^6} \tag{4}$$

This misfit parameter corresponds to the concentration-weighted change of the lattice parameter due to solutes in a solid solution as designated by the conventional theories of solid solution strengthening. Further, $b=\sqrt{2}/2\cdot\sqrt[3]{4\bar{V}}$ is the shortest interatomic distance in the fcc lattice. The misfit parameter eases the comparability of the misfit volume of elements in different alloys and, thus, δ is considered to be a direct measure regarding the materials strength, i.e. an increasing δ is supposed to result in a growing yield stress.

3. Results

3.1. Microstructure

Paramount attention has been paid to get alloys with a single-phase microstructure and precise chemical composition. The chemical compositions of the four-component master alloys are determined by ICP-OES and are given in Tab. 2, indicating a near-equiatomic composition with typical deviations compared to other HEAs. Besides that, the microstructure is set to a recrystallised condition to minimise impacts of texture, grain boundaries and dislocations on the mechanical properties of the alloys. In our previous publication, we have shown that the distribution of crystallographic orientations of polycrystalline AuCuNiPdPt does not show a preferred orientation n the recrystallised state [23]. There is also no distinct texture observed for the microstructure of the presently studied alloys as the samples are in recrystallised condition. Although the magnitude of grain boundaries and dislocations to the strength of the alloys is low, it is of importance that their variation across the 4+x series is kept at a constant level. Scanning electron micrographs in back-scattered electron contrast as well as the corresponding grain sizes of $(CuNiPdPt)_{100-x}Au_x$, $(AuCuPdPt)_{100-x}Ni_x$, $(AuCuNiPt)_{100-x}Pd_x$ and $(AuCuNiPd)_{100-x}Pt_x$ are shown in Fig. 1. Results on the $(AuNiPdPt)_{100-x}Cu_x$ series are published elsewhere [29], and are, therefore, not discussed here again. As can be seen, there are no indications of decomposition, formation of precipitates or secondary phases. Contrast changes (i.e. black spots) within grains and in exceptional cases at grain boundaries were identified as pores which are predominantly caused by the casting process. However, it was not possible to generate the same grain size for all alloys within one 4+x series. Within the 4+x series, the narrowest grain size distribution was found for $(CuNiPdPt)_{100-x}Au_x$ (50 µm to 70 µm) and $(AuCuPdPt)_{100-x}Ni_x$ (30 µm to 50 µm) as shown in Figs. 1(b) and 1(d), respectively. However, the standard deviation of the grain size measurements reveal a more broad size distribution for $(CuNiPdPt)_{100-x}Au_x$ when comparing to $(AuCuPdPt)_{100-x}Ni_x$. In contrast, a significant variation of the grain size is observed for the $(AuCuNiPt)_{100-x}Pd_x$ (10 µm to 50 µm) and $(AuCuNiPd)_{100-x}Pt_x$ (50 µm to 200 µm) series as can be seen from Figs. 1(g) and 1(h), respectively. Due to the very coarse grained microstructure of the $(AuCuNiPd)_{100-x}Pt_x$ alloys, for which a grain size of 100 µm to 200 µm is observed, the influence of Hall-Petch type strengthening is negligible in this subsystem. The $(AuCuNiPt)_{100-x}Pd_x$ alloys exhibit a comparatively high variations of the grain size especially at concentrations of $0 \leq x_{Pd} \leq 10$ at.%. In consequence, the impact of grain boundary strengthening is not at an almost constant level for this series.

The crystal structure and the single-phase constitution was proven by XRD. An exemplary diffraction pattern of the four-component AuCuNiPd alloy is shown in Fig. 2(a). This pattern reveals only reflections that correspond to the Cu structure type. No indications of secondary phases or superlattice reflections can be observed for any of the investigated alloys. Their fcc lattice parameter was refined by means of Rietveld analysis. As shown in Fig 2(b), a linear concentration-dependent behaviour is observed for any of the investigated 4+x series. The validity of Vegard's rule of mixture has already been proven in previous studies [22, 23] and is confirmed here for further compositions within the Au-Cu-Ni-Pd-Pt system. There is no hint that this should not hold for the entire concentrational range.

Due to limited lateral resolution of XRD, there is no reliability regarding the evidence on additional phase(s) of small volume fraction (<5 vol %) and of small length scale from the atomic

scale to the nm-range. However, in view of investigating solid solution strengthening of multicomponent alloys, the presence of a single phase is of tremendous importance to allow a sound verification of the theoretical assumptions. Therefore, atom probe tomography of the four-component equiatomic medium-entropy alloys was utilised for determining the chemical composition and elemental distribution at the atomic level. The results of representative APT analyses are provided in Fig. 3 as well as in Tab. 3. The elemental distribution of the investigated alloys, i.e. CuNiPdPt, AuCuPdPt, AuCuNiPt and AuCuNiPd, appear homogeneous according to the reconstruction of the sample tip. Furthermore, the concentration profiles do not show any significant variations among incremental steps of 1 nm. Even though the measurements indicate a near-equiatomic composition, the values slightly differ from what has been observed by ICP-OES. Possible reasons for this discrepancy are seen in the utilised parameters of the APT measurement, such as temperature and laser energy as well as in inaccuracies during peak decomposition in the analysis.

Regardless that the APT results provide the chemical composition, the experiments were primarily performed to verify the homogeneity of the alloys on the nanometer scale. To exclude the possible formation of nano-scaled clusters due to preferential pairing of elements, a frequency distribution analysis was performed for any APT measurement. For this purpose, the sample tip was sectioned in equi sized volumes of 100 ions each. If elements are randomly distributed within the solid solution, a binomial distribution would be expected. The results are shown in in Fig. 3. Deviations between experimental data and the binomial distribution (solid lines in Figs. 3(c,f,i,l)) are quantified by the Pearson coefficient μ as described in Ref. [24]. This value ranges from 0 to 1, while the random distribution is characterised by $\mu = 0$. The Pearson coefficient of CuNiPdPt, AuCuPdPt and AuCuNiPd amounts to 0.02 to 0.13 (see Tab. 3). The APT measurements of these alloys confirm that they are single phase and that the solid solution is homogeneous. Similar values are observed also for other single phase HEAs [30, 31].

The analysis of AuCuNiPt reveals an increased Pearson coefficients of $\mu_{\mathrm{Au}} = 0.17$, indicating possible cluster formation with an enrichment of this element. Even though the Pearson coefficients of the other elements in this alloy amount to $\mu \lesssim 0.1$, a truly homogeneous distribution of the elements cannot be confirmed without doubt. Based on these results Au may exhibit a small degree of clustering within the solid solution of AuCuNiPt. The size and amount of clustering is below the lateral and chemical resolution limit of APT. It is not further considered in application of the Varvenne model. In consequence, they were supposed to have a minor influence on the mechanical properties, only [14]. Summarising, we have conducted scale-bridging microstructural characterization incl. APT, TEM and SEM. None of the methods have yielded any evidence of secondary phases. We have decided to include SEM for mesoscopic overview and APT for very local chemical fluctuations.

3.2. Mechanical properties of solid solution series

As already mentioned, the theory of Varvenne et al. [4] presently presents the most evolved model for solid solution strengthening. The key parameters of this model are the misfit parameter (cf. Eq. 4) and the mean shear modulus $\bar{G}$ of the alloy. Both parameters depend on the composition of the alloy. Fig. 4 shows their variation across the investigated 4+x series. The value of δ observed for the 4+x series is in the range of 4.2 % to 6.0 %. These values are high, when compared to other HEAs, i.e. CoCrFeMnNi ($\delta = 0.92\,\%$[4]). An increasing content of Au and Ni

within the series $(\mathrm{CuNiPdPt})_{100-x}\mathrm{Au}_x$ and $(\mathrm{AuCuPdPt})_{100-x}\mathrm{Ni}_x$ results in an increase of $\Delta\tau_{\mathrm{c,ss}}$. Contrary, a decreasing trend is observed for $(\mathrm{AuCuNiPt})_{100-x}\mathrm{Pd}_x$ and $(\mathrm{AuCuNiPd})_{100-x}\mathrm{Pt}_x$ with increasing Pd- and Pt-concentration. The mean shear moduli were calculated from the elemental shear moduli by Vegard's rule of mixture and, thus, show a linear behaviour on the fifth element concentration. Based on the trends of δ and $\bar{G}$ as major contributions to $\Delta\tau_{\mathrm{c,ss}}$, differing strengthening behaviours can be expected for the 4+x series as $\delta(x_i)$ and $\bar{G}(x_i)$ show similar as well as dissimilar trends for the individual 4+x series. In fact, the $(\mathrm{AuCuPdPt})_{100-x}\mathrm{Ni}_x$ series is the only one within those under investigation, where both $\delta(x_i)$ and $\bar{G}(x_i)$ show the same trend. Since here the key parameters of the theory of Varvenne et al. [4] rise with increasing concentration, the increase of $\Delta\tau_{\mathrm{c,ss}}(x_i)$ is obvious according to the model.

Without anticipating the results, the following description thereof is divided into a branch at which the experimentally observed mechanical characteristics are in coincidence with the theory of Varvenne et al. [4] as well as a second branch at which modelling fails. In any case, the effect of solutes on the mechanical properties of the alloys is characterised by the hardness, the yield stress as well as the 0.07 flow stress. These values are shown for each 4+x series and are compared to the contribution of solid solution strengthening according to the theory of Varvenne et al. [4]. Since δ has been identified as the major contribution to $\Delta\sigma_{\mathrm{c,ss}}$, a second abscissa depicting the x_i-correlated values of the δ parameter is also shown.

3.2.1. Concurrent scaling behaviour of $\sigma_y(x_i)$ and $\Delta\sigma_{c,ss}(x_i)$

The mechanical properties of the $(\mathrm{AuCuPdPt})_{100-x}\mathrm{Ni}_x$ series are shown in Fig. 5(c). The yield stress σ_y increases almost linearly with the Ni concentration x_{Ni} in this 4+x series. All samples are measured in the recrystallised condition. Therefore, the dislocation density in these alloys is at a comparable low level and the contribution of work hardening to σ_y remains constant and at a low level across this series. Although no values can be given for this contribution to σ_y, the observed trend would not be affected. The same holds for grain boundary strengthening. As can be seen from Fig. 1(b) and (f) the grain sizes of the alloys are almost constant. The influence of grain boundary strengthening was estimated with a Hall-Petch coefficient of $0.675\,\mathrm{MPa}/\sqrt{\mathrm{m}}$, which has been determined for AuCuNiPdPt [23]. According to the maximum difference of the grain size of alloys from the $(\mathrm{AuCuPdPt})_{100-x}\mathrm{Ni}_x$ series ($\Delta D = 20\,\mu\mathrm{m}$) the contribution to grain boundary strengthening would show a variation of only 23 MPa, which is in the order of the symbol size of Fig. 5(c). Grain boundary strengthening is negligible for the present analysis of solid solution strengthening in this series. This is additionally shown by the hardness values, whose influence by the grain size in µm-range is almost negligible. In fact, hardness and 0.07 flow stress, which are related to each other [32] show the same linear trend as the σ_y values. Hence, also the impact of the grain size on the yield stress of these alloys is negligible and the shown values and in particular the rise of $\sigma_y(x_{\mathrm{Ni}})$ are caused by solid solution strengthening.

The contribution of solid solution strengthening $\Delta\sigma_{\mathrm{c,ss}}$ to the yield stress according to the theory of Varvenne et al. [4] is depicted in Fig. 5(d) for the $(\mathrm{AuCuPdPt})_{100-x}\mathrm{Ni}_x$ series. As can be seen, the $\Delta\sigma_{\mathrm{c,ss}}$ values linearly increase with x_{Ni}. The same trend is observed when $\Delta\sigma_{\mathrm{c,ss}}$ is plotted in dependence on the key misfit parameter δ. However, when considering the absolute values, the increase of $\Delta\sigma_{\mathrm{c,ss}}$ from AuCuPdPt to AuCuNiPdPt is considerably lower, i.e. 200 MPa when comparing to the increase of the experimentally observed σ_y values, 400 MPa. Possible reasons for this discrepancy can be e.g. a variation of the proof stress or the stacking

fault energy across this series violating the basic assumption that all contributors to the yield stress besides that arising from solid solution strengthening are at the same level. Alternatively, or in addition to these issues, the formation of preferred next neighbours might also vary across this series providing a further, yet unresolved contribution to σ_y. However, there are currently no indications that these changes in the microstructure occur. In addition, possible minor deviations between experiment and theory might be induced by the sensitivity of the model regarding its input parameters. Among all investigated 4+x series, $(\mathrm{AuCuPdPt})_{100-x}\mathrm{Ni}_x$ shows by far the most homogeneous variation of the microstructure across the whole series. In consequence of this and due to the fact that x_{Ni} and δ are linearly correlated the variation of the mechanical properties can well be modelled according to the theory of Varvenne et al. [4].

The experimentally observed mechanical properties of the $(\mathrm{CuNiPdPt})_{100-x}\mathrm{Au}_x$ series are very similar to those of the previously presented $(\mathrm{AuCuPdPt})_{100-x}\mathrm{Ni}_x$ series, see Fig. 5(a). The microstructural parameters of this series also do not indicate any significant deviation from this behaviour. According to the sizes of the elements (Ni is the smallest and Au the largest atom within the Au-Cu-Ni-Pd-Pt alloys) the δ parameter increases from the four-component alloy to the equiatomic five component alloy. As shown in Fig. 5(b), $\Delta\sigma_{\mathrm{c,ss}}$ of $(\mathrm{CuNiPdPt})_{100-x}\mathrm{Au}_x$ increases with increasing Au concentration. In contrast to the previous results, the tendency is non-linear, yielding to a lower strengthening effect of Au in this series at high x_{Au} values. This image of a non-linear trend of $\Delta\sigma_{\mathrm{c,ss}}$ must be considered in the context that strength does not only depend on δ but also on the shear modulus. In the case of $(\mathrm{CuNiPdPt})_{100-x}\mathrm{Au}_x$, the shear modulus decreases with increasing concentration, while in the Ni series it increases with x_i. Thus, while the $(\mathrm{AuCuPdPt})_{100-x}\mathrm{Ni}_x$ series shows a concurrent scaling of $\delta(x_{\mathrm{Ni}})$ and $G(x_{\mathrm{Ni}})$, the corresponding scaling in the case of the $(\mathrm{CuNiPdPt})_{100-x}\mathrm{Au}_x$ series is of opposite sign.

The increasing trend of the yield stress is in principle also reproduced by the theory of Varvenne et al. [4]. However, neither the dependency on the composition, $\delta(x_{\mathrm{Au}})$ nor the absolute change of the contribution to the strength are in agreement with the experimental values. It should be noted that although $\Delta\sigma_{\mathrm{c,ss}}$ of the $(\mathrm{CuNiPdPt})_{100-x}\mathrm{Au}_x$ and $(\mathrm{AuCuPdPt})_{100-x}\mathrm{Ni}_x$ series increase with δ, the respective slopes are clearly different. The difference in $\Delta\sigma_{\mathrm{c,ss}}$ between AuCuNiPdPt and an alloy with $\delta = 4.6$ is roughly twice as large as in the $(\mathrm{AuCuPdPt})_{100-x}\mathrm{Ni}_x$ series. At present, apart from the previous speculations, there are no explanations for this mismatch. However, these experiments demonstrate that the assumptions of Varvenne et al. [4] being made to assess solid solution strengthening in multicomponent alloys like HEAs are correct in essence and that the theory can provide a sound behaviour which is consistent with the experiment.

3.2.2. $\sigma_y(x_i)$ behaviour inexplicable by theory

In our previous publication, a breakdown of the scaling of σ_y according to the theory of Varvenne et al. [4] has been observed in the $(\mathrm{AuNiPdPt})_{100-x}\mathrm{Cu}_x$ series [29]. In this case, the $\Delta\sigma_{\mathrm{c,ss}}(x_{\mathrm{Cu}})$ values show a slight non-linear increase with increasing x_{Cu} (approx. 20 MPa), while $\sigma_y(x_{\mathrm{Cu}})$ decreases linearly but significantly (approx. 500 MPa) between AuNiPdPt and the five component equiatomic alloy. The mechanical properties of the $(\mathrm{AuCuNiPt})_{100-x}\mathrm{Pd}_x$ and $(\mathrm{AuCuNiPd})_{100-x}\mathrm{Pt}_x$ series are shown in Fig. 6 in dependence of the chemical composition x_i and δ (upper abscissae). In these two cases, δ decreases with increasing x_i. Therefore, the visualisation of $\Delta\sigma_{\mathrm{c,ss}}(x_i)$ in Fig. 6 appears falling in dependence of x_i but rising when referring

to δ.

The $(\mathrm{AuCuNiPd})_{100-x}\mathrm{Pt}_x$ series shows a linear increase of $\sigma_y(x_{\mathrm{Pt}})$, which is also reflected by the behaviour of the hardness and the 0.07 flow stress. Although the average grain sizes of the individual alloys in this series vary, their absolute values are comparably high. In consequence the contribution of grain boundary strengthening to the total strength is apparently low. Assuming the Hall-Petch constant of the HEA to be valid for the whole $(\mathrm{AuCuNiPd})_{100-x}\mathrm{Pt}_x$ series yields contributions from grain boundary strengthening to the total strength between 50 MPa and 90 MPa. Hence, the corresponding variation across this series is approx. 40 MPa, which is the 1.6-fold of the symbol size in Fig. 6(a). The total increase of σ_y between AuCuNiPd and the HEA is comparable to the previously discussed series, i.e. approx. 400 MPa, which means that the effect of grain boundary strengthening has a minor influence, only. Fig. 6(b) depicts the course of $\Delta\sigma_{\mathrm{c,ss}}(x_{\mathrm{Pt}})$, which in contrast to the experimental values shows a decreasing trend. In addition, the drop of $\Delta\sigma_{\mathrm{c,ss}}$ between AuCuNiPd and the HEA amounts to approx. 30 MPa. When comparing this to the experimentally observed strength values, it becomes obvious, that both, the slope as well as the total change cannot be explained within the model of Varvenne et al. [4].

The prediction of the yield stress due to the model of Varvenne et al. [4] is also not in agreement with the experimental trends of the mechanical properties of the $(\mathrm{AuCuNiPt})_{100-x}\mathrm{Pd}_x$ series. However, the analysis is more complicated here since the grain size varies significantly across this series. This causes a varying and, thus non-constant contribution of grain boundary strengthening to the total strength, which results in a larger scatter of the values of σ_y and the 0.07 flow stress when compared to other 4+x series. This contribution ranges from 95 MPa to 192 MPa when assuming that the Hall-Petch coefficient of AuCuNiPdPt is valid for the whole $(\mathrm{AuCuNiPt})_{100-x}\mathrm{Pd}_x$ series. As the overall change of σ_y is apparently low, the varying contribution of grain boundary strengthening significantly affects its trend across this 4+x series. In contrast to that, the variation of the Pd concentration does not essentially affect the Vickers microhardness of the $(\mathrm{AuCuNiPt})_{100-x}\mathrm{Pd}_x$ series within the range of 0.2 at.% to 20 at.%. The microhardness is virtually insensitive to the grain size in the µm-range and since it virtually does not change within the $(\mathrm{AuCuNiPt})_{100-x}\mathrm{Pd}_x$ series, it can be assumed that an almost unchanged trend of the mechanical response is representative for this series. Also with regard to the variation of σ_y, this 4+x series appears special. While the change in σ_y is large for the other series (approx. 400 MPa), the strength of AuCuNiPt and AuCuNiPdPt are virtually the same. In between these two alloys, the $(\mathrm{AuCuNiPt})_{100-x}\mathrm{Pd}_x$ series does not provide a clear image of the trend of $\sigma_y(x_{\mathrm{Pd}})$ but a large scatter, which is in the same order as the difference between the individual contributions of grain boundary strengthening to the total strength. Further, a slight effect of element clustering cannot be completely excluded.

$\Delta\sigma_{\mathrm{c,ss}}(x_{\mathrm{Pd}})$ according to the model of Varvenne et al. [4] is shown in Fig. 6(d) for the $(\mathrm{AuCuNiPt})_{100-x}\mathrm{Pd}_x$ series. A linear decrease is observed with increasing x_{Pd}, which in addition is significant when compared to the other series, i.e. a loss in $\Delta\sigma_{\mathrm{c,ss}}$ of 120 MPa has been calculated when comparing AuCuNiPt to AuCuNiPdPt. Also in this case, theory drafts a correlation between the strength and the key misfit parameter. However, this scaling behaviour cannot be confirmed by the present experiments.

4. Discussion

Samples within the Au-Cu-Ni-Pd-Pt system are single-phase. Therefore, as outlined before, this system is capable of making composition dependent investigations of mechanical properties without the necessity to in-depth analyse other strengthening effects, such as precipitation strengthening. Dislocation strengthening is kept at a comparable but low level, as investigations were made for the recrystallised state. Only the grain size was not be kept at the same level and, thus, Hall-Petch type hardening occurs at a varying amount. Due to the size and its variation, grain boundary strengthening has been shown to have a minor influence on the overall variation of the strength values of the investigated series assuming that the Hall-Petch coefficient thereof does not significantly differ from that of AuCuNiPdPt. As the hardness is not sensitive to the grain size, the overall trend of the strength is substantiated. Small deviations of the strength values from the observed trends that are not seen in the hardness values can be explained by an alteration of the grain size. As the microstructural investigations do not reveal any secondary phases or segregations, the variation of the observed strength values within the investigated alloy series are discussed as if they were dependent only on solid solution hardening.

From the comparison of the experimental data of the mechanical properties of the 4+x series to the calculated contribution of solid solution strengthening to the total strength, $\Delta\sigma_{c,ss}(x_i)$, as shown in Figs.5 and 6 no clear conclusive evaluation can be drawn because on the one hand a concurrent scaling behaviour of $\sigma_y(x_i)$ and $\Delta\sigma_{c,ss}(x_i)$ is observed and on the other hand there are 4+x series for whose the observed mechanical behaviour cannot be described on the basis of the model by Varvenne et al. [4]. In detail and as already pointed out, the trend of $\Delta\sigma_{c,ss}(x_i)$ is not in agreement with the experimental data for $(\mathrm{AuCuNiPt})_{100-x}\mathrm{Pd}_x$, $(\mathrm{AuCuNiPd})_{100-x}\mathrm{Pt}_x$ and $(\mathrm{AuNiPdPt})_{100-x}\mathrm{Cu}_x$ [29]. As depicted in Fig. 6(b) and 6(d), in both cases a nearly linear decrease of $\Delta\sigma_{\mathrm{c,ss}}(x_i)$ would be expected from theory. It should be noted, that in both cases, the trends of $\Delta\sigma_{\mathrm{c,ss}}$ are in the opposite direction, when being regarded in dependence of (x_i) or δ. This is obvious from Fig. 4, since δ and x_i are not correlated across different 4+x series and a decreasing δ parameter is seen for increasing x_i. According to the theory, $\Delta\sigma_{\mathrm{c,ss}}(\delta)$ always rises, but in the present article the composition is given due to the faced discrepancies in the $(\mathrm{AuCuNiPd})_{100-x}\mathrm{Pt}_x$ and $(\mathrm{AuNiPdPt})_{100-x}\mathrm{Cu}_x$ (not shown here, please refer to [29]) series.

In contrast to the $(\mathrm{AuCuNiPt})_{100-x}\mathrm{Pd}_x$ and $(\mathrm{AuCuNiPd})_{100-x}\mathrm{Pt}_x$ series, the general trends for $(\mathrm{CuNiPdPt})_{100-x}\mathrm{Au}_x$ and $(\mathrm{AuCuPdPt})_{100-x}\mathrm{Ni}_x$ correspond reasonable well with the theory of Varvenne et al. [4]. While for the $(\mathrm{AuCuPdPt})_{100-x}\mathrm{Ni}_x$ series both parameters, δ and G show the largest rise across the series it appears obvious, that the largest change of $\Delta\sigma_{\mathrm{c,ss}}(x_i)$ is predicted. This series shows the best agreement between experimental values of the variation of the strength across the series and the variation of the theoretically determined $\Delta\sigma_{\mathrm{c,ss}}$. In all other cases, the change of the parameters, δ and G are either less pronounced, or of opposed sign, or both. These opposite trends of the misfit parameter δ and the shear modulus G as a function of x_i (cf. Fig. 4(b)) might have a very minor effect on the scaling behaviour of $\Delta\sigma_{\mathrm{c,ss}}$. Furthermore, the calculation of the contribution of solid solution strengthening upon the model of Varvenne et al. [4] is based on the average determination of input parameters from elemental properties, i.e. lattice parameter, shear modulus, Poisson's ratio and stable/unstable stacking fault energies. All of these quantities depend on the composition, but are well-defined average quantities [1]. As proved in Fig. 2(b) utilisation of Vegard's rule of mixture is valid for lattice parameters of alloys

within the Au-Cu-Ni-Pd-Pt system [22]. However, e.g. the shear modulus must not necessarily follow this rule. It has been shown, that this is not the case for binary systems, i.e. $Au_{50}Pd_{50}$ and $Cu_{50}Ni_{50}$ with a maximum deviation of 20 % and 7 %, respectively, compared to the linear superposition according to Vegard's rule of mixture [33]. Further research is required to obtain reliable values for the shear modulus across the investigated series to address this open question.

A further issue is based on the parameter conception of Varvenne et al. [4, 9] regarding ΔV and $\bar{G}$. Solutes are seen as additional atoms with different lattice spacing and shear modulus introduced in the solvent matrix resulting in a modification of the aforementioned parameters [6]. This implicitly affects local misfit strains and hence, is directly related to solid solution strengthening. However, this can be misleading, because the averaged macroscopic misfit volume must not be necessarily equal to the local volume change nor correlate to the lattice distance between nearest neighbours [6]. If volume changes are high, which is the case for Au-Cu-Ni-Pd-Pt, this issue could gain crucial relevance. Due to the sensitivity of the model regarding the input parameters, this results in deceptive strengthening predictions. Moreover, a local variation of the parameters ΔV and $\bar{G}$ caused by nearest-neighbour correlations is expected to result in the deviation compared to the global wide-ranging values.

At this point, the present experimental data can be the key to further enhance the models of solid solution strengthening. One of the assumptions of the model is that there is an effective matrix in which atoms are considered as dilute atoms. The model of C. Varvenne [1] has been proven against binary alloys in the dilute limit as well as against the CoCrFeMnNi HEA and subsystems thereof. In both cases, the matrix does not face severe volume changes, as e.g. the atomic sizes of Co, Cr, Fe, Mn and Ni are similar. In fact, the atomic sizes in the CoCrFeMnNi alloy show a standard deviation of 6.8 pm and a δ parameter of 0.016. In contrast, the standard deviation of the atomic radii in the AuCuNiPdPt alloy is higher, i.e. 14.7 pm and the δ parameter amounts to 0.053. Presently, there is no experimental prove of the properties of the average matrix and the model does not provide direct insights into it, the solute properties, or the overall composition [1].

The presently investigated 4+1 series can be utilised to improve the model for solid solution strengthening of multi-component alloys. In contrast to modelling the solid solution strengthening of various equi-molar alloys in the Co-Cr-Fe-Mn-Ni system, the modelling for dilute elements with different amounts in equi-molar multi-component alloys become possible upon an experimental data base. The matrix atoms always have a high concentration, while the solution is varied from a dilute solution to the equi-molar composition. This model would need to consider significant distortions of the dislocation core structure of the (effective) matrix material. In multi-component alloys, the random distribution of atoms cause lattice distortions and variations of strength of the binding which can be described as an energy landscape in which dislocations move. It would be needed to address the line-tension parameter α for alloys. The experimental and theoretical basis for the evaluation of this parameter requires substantiation. Unfortunately, the line-tension parameter α is treated as a constant for HEAs, which presumably is not the case.

The investigated alloys were thoroughly processed and are single-phase samples, which is observed over a wide range of the length scale. However, the unambiguous evidence of a single-phase state in multicomponent, highly concentrated alloys is experimentally infeasible with manageable effort. This is caused by the combined lateral and chemical resolution limits of microscopic

techniques, ranging from µm- (XRD, SEM) to the nm-scale (APT). Nevertheless, short-range order or elemental clustering within the extent of several unit cells and consequently, further strengthening mechanisms cannot be completely excluded. However, a reverse trend of the mechanical properties due to their possible appearance should not be expected [12, 14]. Although we cannot provide an explanation for the observed trends and further work is needed to resolve the addressed open questions, we believe the principal results, summarised in the conclusions, are worth publishing immediately.

5. Conclusions

We put considerable efforts in obtaining $(ABCD)_{100-x}E_x$ samples from Au, Cu, Ni, Pd and Pt that are ideal in the sense that their mechanical properties are predominately influenced by solid solution strengthening. This means that dislocation strengthening and grain boundary strengthening are minimised and other strengthening effects, such as secondary phases or ordering are not detected within the limitations of the experiments. The mentioned series within the Au-Cu-Ni-Pd-Pt system are capable of validating existing models for solid solution strengthening in highly concentrated alloys, as adjustments in the chemical composition do not alter the single-phase nature of this alloy.

On the μm-scale, all investigated alloys exhibit a homogeneous, single phase, fcc microstructure. This was also confirmed on the nm-scale by APT measurements for CuNiPdPt, AuCuPdPt and AuCuNiPd, however, AuCuNiPt exhibit initial indications for element clustering. The mechanical behaviour in case of microhardness and compressive yield stress and flow stress at 0.07 true strain reveals three different scenarios: *(i)* linear increasing of the strength for $(CuNiPdPt)_{100-x}Au_x$, $(AuCuPdPt)_{100-x}Ni_x$ and $(AuCuNiPd)_{100-x}Pt_x$, *(ii)* constant strength for $(AuCuNiPt)_{100-x}Pd_x$ and *(iii)* linear decreasing strength for $(AuNiPdPt)_{100-x}Cu_x$ (published in Ref. [29]). Even though it was not possible to unambiguously clarify the correlation between the mechanical behaviour and possible inhomogeneities, however, a considerable deviation of the trends is not expected.

The yield stress predicted by the model of Varvenne et al. [4, 9] merely shows a sound tendency for $(CuNiPdPt)_{100-x}Au_x$ and $(AuCuPdPt)_{100-x}Ni_x$, whereas an opposite trend was observed for $(AuCuNiPt)_{100-x}Pd_x$ and $(AuCuNiPd)_{100-x}Pt_x$. Assuming that the mechanical strength of the alloys is not influenced by additional mechanisms and that the shown trends of the strength in dependence on the composition of the alloy are valid even in the case that unresolved features having minor effects on the general trends, the discrepancy between experiment and model is obvious in some cases. Further work to substantiate models for solid solution strengthening appears to be needed and the present results may be used as benchmark to evaluate these models.

Acknowledgement

This work was supported by the Deutsche Forschungsgemeinschaft (DFG) within the priority programme *Compositionally Complex Alloys – High-Entropy Alloys (CCA-HEA)* (SPP 2006, grant nos. FR 1714/7-1 (FT, JF), KA 4631/1-1 (AK) and STU 611/2-1 (DU, KA)). This financial support is greatfully acknowledged. This work was partly carried out with the support of the

Karlsruhe Nano Micro Facility (KNMF, www.knmf.kit.edu), a Helmholtz Research Infrastructure at Karlsruhe Institute of Technology (KIT, www.kit.edu). Furthermore, we would like to express our gratitude to A. Voss, M.J. Kriegel, D. Seifert, C. Bollnow, S. Donath, B. Gebel, J. Scheiter, and K. Schröder for experimental support.

Data Availability

The raw data as well as the processed data required to reproduce these findings are available from the corresponding author upon request.

References

[1] C. Varvenne, G. P. M. Leyson, M. Ghazisaeidi, W. A. Curtin, Solute strengthening in random alloys, Acta Materialia 124 (2017) 660 – 683. doi:10.1016/j.actamat.2016.09.046.

[2] J.-W. Yeh, S.-K. Chen, S.-J. Lin, J.-Y. Gan, T.-S. Chin, T.-T. Shun, C.-H. Tsau, S.-Y. Chang, Nanostructured High-Entropy Alloys with Multiple Principal Elements: Novel Alloy Design Concepts and Outcomes, Advanced Engineering Materials 6 (2004) 299–303. doi:10.1002/adem.200300567.

[3] B. Cantor, I. T. H. Chang, P. Knight, A. J. B. Vincent, Microstructural development in equiatomic multicomponent alloys, Materials Science and Engineering: A 375-377 (2004) 213 – 218. doi:10.1016/j.msea.2003.10.257.

[4] C. Varvenne, A. Luque, W. A. Curtin, Theory of strengthening in fcc high entropy alloys, Acta Materialia 118 (2016) 164 – 176. doi:10.1016/j.actamat.2016.07.040.

[5] N. L. Okamoto, K. Yuge, K. Tanaka, H. Inui, E. P. George, Atomic displacement in the CrMnFeCoNi high-entropy alloy A scaling factor to predict solid solution strengthening, AIP Advances 6 (2016) 125008. doi:10.1063/1.4971371.

[6] E. P. George, W. A. Curtin, C. C. Tasan, High entropy alloys: A focused review of mechanical properties and deformation mechanisms, Acta Materialia 188 (2020) 435 – 474. doi:10.1016/j.actamat.2019.12.015.

[7] R. Labusch, A Statistical Theory of Solid Solution Hardening, physica status solidi (b) 41 (1970) 659–669. doi:10.1002/pssb.19700410221.

[8] D. B. Miracle, O. N. Senkov, A critical review of high entropy alloys and related concepts, Acta Materialia 122 (2017) 448 – 511. doi:10.1016/j.actamat.2016.08.081.

[9] C. Varvenne, W. A. Curtin, Predicting yield strengths of noble metal high entropy alloys, Scripta Materialia 142 (2018) 92 – 95. doi:10.1016/j.scriptamat.2017.08.030.

[10] F. X. Zhang, S. Zhao, K. Jin, H. Xue, G. Velisa, H. Bei, R. Huang, J. Y. P. Ko, D. C. Pagan, J. C. Neuefeind, W. J. Weber, Y. Zhang, Local Structure and Short-Range Order in a NiCoCr Solid Solution Alloy, Physical Review Letters 118 (2017) 205501. doi:10.1103/PhysRevLett.118.205501.

[11] R. Zhang, S. Zhao, J. Ding, Y. Chong, T. Jia, C. Ophus, M. Asta, R. O. Ritchie, A. M. Minor, Short-range order and its impact on the CrCoNi medium-entropy alloy, Nature 581 (2020) 283–287. doi:10.1038/s41586-020-2275-z.

[12] B. Yin, S. Yoshida, N. Tsuji, W. A. Curtin, Yield strength and misfit volumes of NiCoCr and implications for short-range-order, Nature Communications 11 (2020) 2507. doi:10.1038/s41467-020-16083-1.

[13] H. Chen, A. Kauffmann, S. Seils, T. Boll, C. H. Liebscher, I. Harding, K. S. Kumar, D. V. Szab, S. Schlabach, S. Kauffmann-Weiss, F. Mller, B. Gorr, H.-J. Christ, M. Heilmaier, Crystallographic ordering in a series of Al-containing refractory high entropy alloys TaNbMoCrTiAl, Acta Materialia 176 (2019) 123 – 133. doi:10.1016/j.actamat.2019.07.001.

[14] B. Yin, W. A. Curtin, Origin of high strength in the CoCrFeNiPd high-entropy alloy, Materials Research Letters 8 (2020) 209–215. doi:10.1080/21663831.2020.1739156.

[15] E. Antillon, C. Woodward, S. I. Rao, B. Akdim, T. A. Parthasarathy, Chemical short range order strengthening in a model fcc high entropy alloy, Acta Materialia 190 (2020) 29 – 42. doi:https://doi.org/10.1016/j.actamat.2020.02.041.

[16] T. Keil, E. Bruder, K. Durst, Exploring the compositional parameter space of high-entropy alloys using a diffusion couple approach, Materials & Design (2019) 107816doi:10.1016/j.matdes.2019.107816.

[17] M. Laurent-Brocq, L. Perrire, R. Pirs, Y. Champion, From high entropy alloys to diluted multi-component alloys: Range of existence of a solid-solution, Materials & Design 103 (2016) 84 – 89. doi:10.1016/j.matdes.2016.04.046.

[18] M. Laurent-Brocq, L. Perrire, R. Pirs, F. Prima, P. Vermaut, Y. Champion, From diluted solid solutions to high entropy alloys: On the evolution of properties with composition of multi-components alloys, Materials Science and Engineering: A 696 (2017) 228 – 235. doi:10.1016/j.msea.2017.04.079.

[19] G. Bracq, M. Laurent-Brocq, C. Varvenne, L. Perrire, W. A. Curtin, J.-M. Joubert, I. Guillot, Combining experiments and modeling to explore the solid solution strengthening of high and medium entropy alloys, Acta Materialia 177 (2019) 266 – 279. doi:10.1016/j.actamat.2019.06.050.

[20] C. Varvenne, W. A. Curtin, Strengthening of high entropy alloys by dilute solute additions: $CoCrFeNiAl_x$ and $CoCrFeNiMnAl_x$ alloys, Scripta Materialia 138 (2017) 92 – 95. doi:10.1016/j.scriptamat.2017.05.035.

[21] B. Yin, W. A. Curtin, First-principles-based prediction of yield strength in the RhIrPdPt-NiCu high-entropy alloy, npj Computational Materials 5 (2019) 14. doi:10.1038/s41524-019-0151-x.

[22] J. Freudenberger, D. Rafaja, D. Geissler, L. Giebeler, C. Ullrich, A. Kauffmann, M. Heilmaier, K. Nielsch, Face Centred Cubic Multi-Component Equiatomic Solid Solutions in the Au-Cu-Ni-Pd-Pt System, Metals 7 (2017) 135. doi:10.3390/met7040135.

[23] F. Thiel, D. Geissler, K. Nielsch, A. Kauffmann, S. Seils, M. Heilmaier, D. Utt, K. Albe, M. Motylenko, D. Rafaja, J. Freudenberger, Origins of strength and plasticity in the precious metal based high-entropy alloy AuCuNiPdPt, Acta Materialia 185 (2020) 400 – 411. doi:10.1016/j.actamat.2019.12.020.

[24] M. P. Moody, L. T. Stephenson, A. V. Ceguerra, S. P. Ringer, Quantitative binomial distribution analyses of nanoscale like-solute atom clustering and segregation in atom probe tomography data, Microscopy Research and Technique 71 (2008) 542–550. doi:10.1002/jemt.20582.

[25] D. Larson, T. Prosa, R. Ulfig, B. Geiser, T. Kelly, Local Electrode Atom Probe Tomography, Springer-Verlag New York, 2013. doi:10.1007/978-1-4614-8721-0.

[26] B. Szajewski, F. Pavia, W. Curtin, Robust atomistic calculation of dislocation line tension, Modelling and Simulation in Materials Science and Engineering 23 (2015) 085008. doi:https://doi.org/10.1088/0965-0393/23/8/085008.

[27] L. Vegard, Die Konstitution der Mischkristalle und die Raumfüllung der Atome, Zeitschrift für Physik 5 (1921) 17–26. doi:10.1007/BF01349680.

[28] T. Gray, Periodic table, http://www.periodictable.com, accessed: 05-May-2022.

[29] F. Thiel, D. Utt, A. Kauffmann, K. Nielsch, K. Albe, M. Heilmaier, J. Freudenberger, Breakdown of Varvenne scaling in $(AuNiPdPt)_{1-x}Cu_x$ high-entropy alloys, Scripta Materialia 181 (2020) 15–18. doi:10.1016/j.scriptamat.2020.02.007.

[30] M. Vaidya, K. G. Pradeep, B. S. Murty, G. Wilde, S. V. Divinski, Bulk tracer diffusion in CoCrFeNi and CoCrFeMnNi high entropy alloys, Acta Materialia 146 (2018) 211 – 224. doi:10.1016/j.actamat.2017.12.052.

[31] C. Lee, G. Song, M. C. Gao, R. Feng, P. Chen, J. Brechtl, Y. Chen, K. An, W. Guo, J. D. Poplawsky, S. Li, A. T. Samaei, W. Chen, A. Hu, H. Choo, P. K. Liaw, Lattice distortion in a strong and ductile refractory high-entropy alloy, Acta Materialia 160 (2018) 158 – 172. doi:10.1016/j.actamat.2018.08.053.

[32] K. L. Johnson, Contact Mechanics, Cambridge University Press, 1985.

[33] W. Köster, W. Rauscher, Beziehungen zwischen den Elastizitätsmodulen von Zweistoffegierungen und deren Aufbau, Zeitschrift für Metallkunde 39 (1948) 111–114.

Table 1: Input data of the properties for the pure elements contained in the HEA provided by Wolfram Research (2007), ElementData, Wolfram Language function, https://reference.wolfram.com/language/ref/ElementData.html. a_0 is the fcc lattice constant, E the Young's modulus, and G the shear modulus.

Element	a_i/nm	G/GPa	E/GPa
Au	0.40782	27	78
Cu	0.36149	48	130
Ni	0.35240	76	200
Pd	0.38907	44	121
Pt	0.39242	61	168

Table 2: Chemical composition of the master alloys as determined by ICP-OES. Values are given in at.%. The Pt content in the AuCuNiPd alloy arises from contamination.

alloy	Au	Cu	Ni	Pd	Pt
CuNiPdPt	–	24.88±0.10	25.07±0.16	24.78±0.12	25.27±0.15
AuNiPdPt	25.11±0.46	–	25.03±0.84	24.93±0.42	24.92±0.10
AuCuPdPt	24.82±0.39	24.68±0.19	–	25.00±0.10	25.49±0.34
AuCuNiPt	25.44±1.36	25.01±0.52	24.66±1.00	–	24.89±1.22
AuCuNiPd	25.18±0.20	24.80±0.08	24.91±0.14	24.90±0.11	0.21±0.05

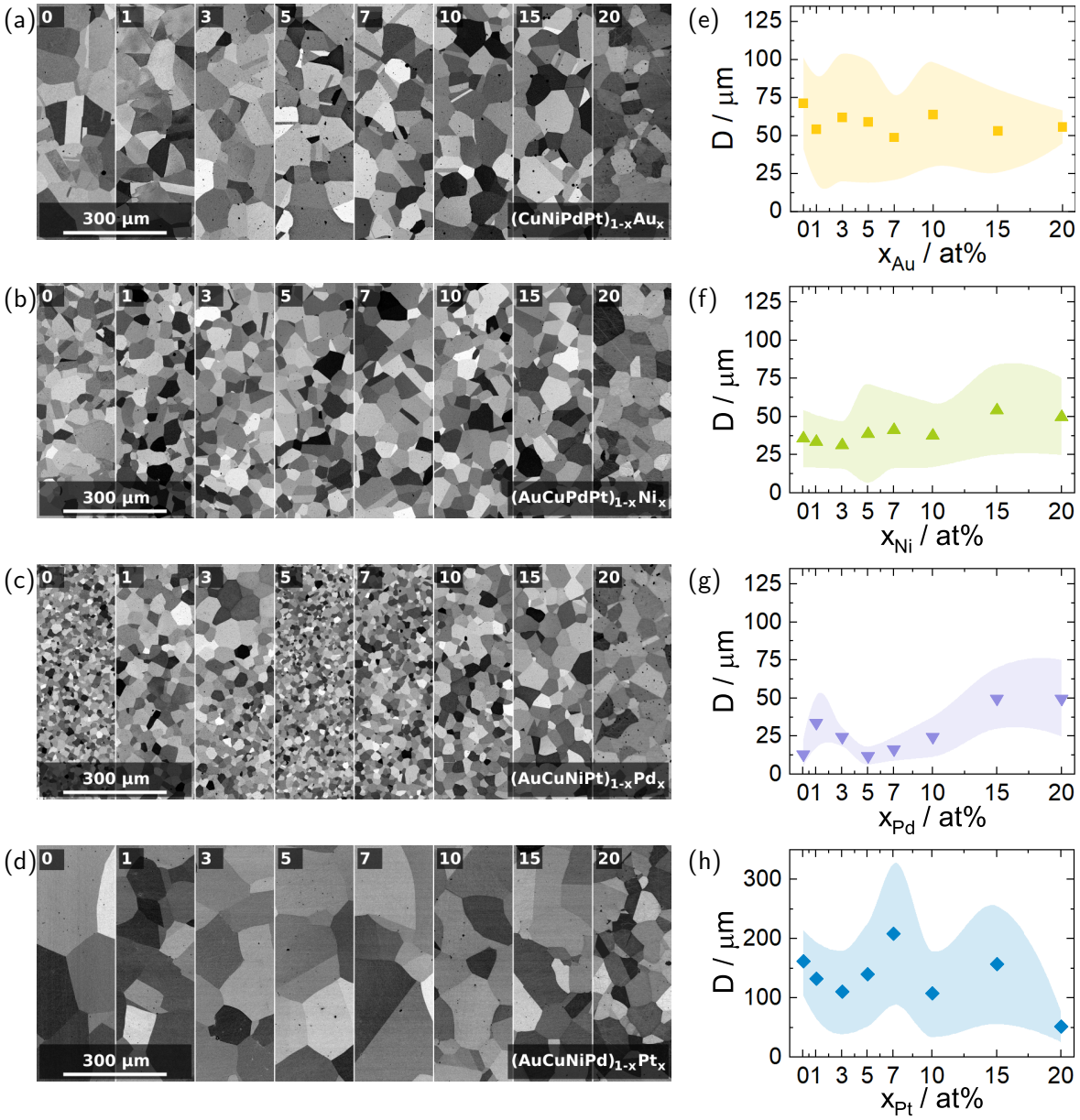

Figure 1: Microstructure characterisation of solid solution series: (a)–(d) scanning electron micrographs (back-scattered electron contrast) of alloys as denoted in the corresponding figure in the recrystallised state. The scaling bar accounts for all micrographs and the depicted number accounts for the corresponding content of the varying component. (e)–(h) grain size in dependence of the chemical composition. For better comparability the scale of y-axis in (h) was expanded.

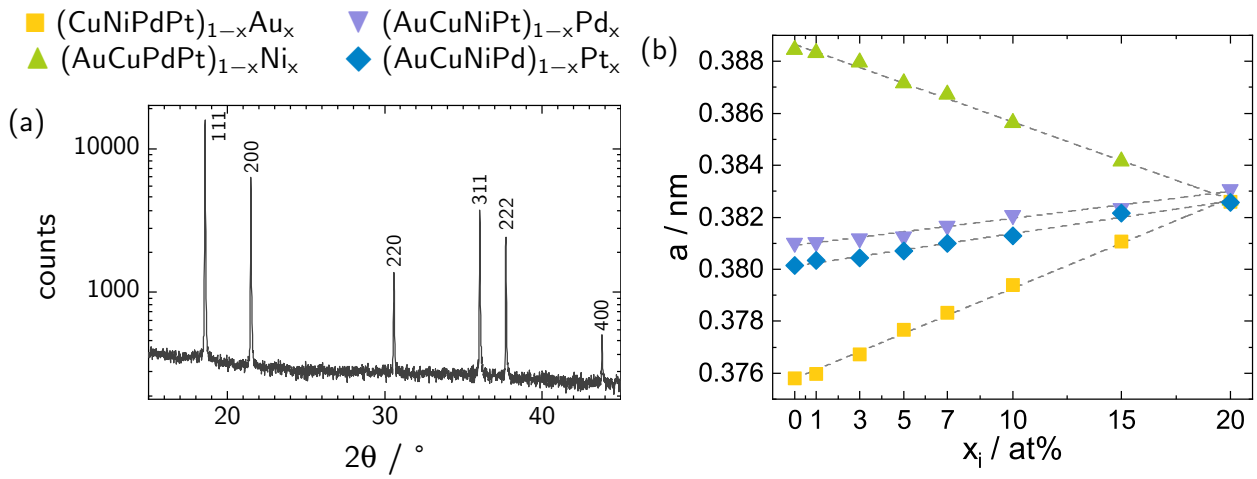

Figure 2: X-ray diffraction: (a) exemplary XRD pattern of AuCuNiPd in the recrystallised state and (b) lattice parameters of the solid solution series depending on the chemical composition.

Table 3: Mean chemical composition of the four-component alloys CuNiPdPt, AuCuPdPt, AuCuNiPt and AuCuNiPd in the recrystallised state determined by means of APT. The Pearson-coefficient μ is a measure of the deviation of the theoretical binomial distribution and the experimental data of the elemental concentration distribution within the analysed volume of 100 ions.

Element	Au	Cu	Ni	Pd	Pt
CuNiPdPt	–	22.20±0.26	28.70±0.26	22.03±0.65	26.93±0.7
μ	–	0.06±0.01	0.05±0.01	0.08±0.03	0.07±0.04
AuCuPdPt	21.72±0.69	24.98±0.75	–	26.06±0.44	27.16±0.49
μ	0.10±0.03	0.03±0.01	–	0.03±0.01	0.13±0.02
AuCuNiPt	21.73±0.44	23.83±0.20	27.46±0.27	–	26.83±0.38
μ	0.19±0.04	0.08±0.01	0.14±0.02	–	0.09±0.03
AuCuNiPd	21.83±0.81	25.27±0.41	26.84±0.70	25.65±0.26	–
μ	0.09±0.03	0.06±0.05	0.07±0.02	0.02±0.01	–

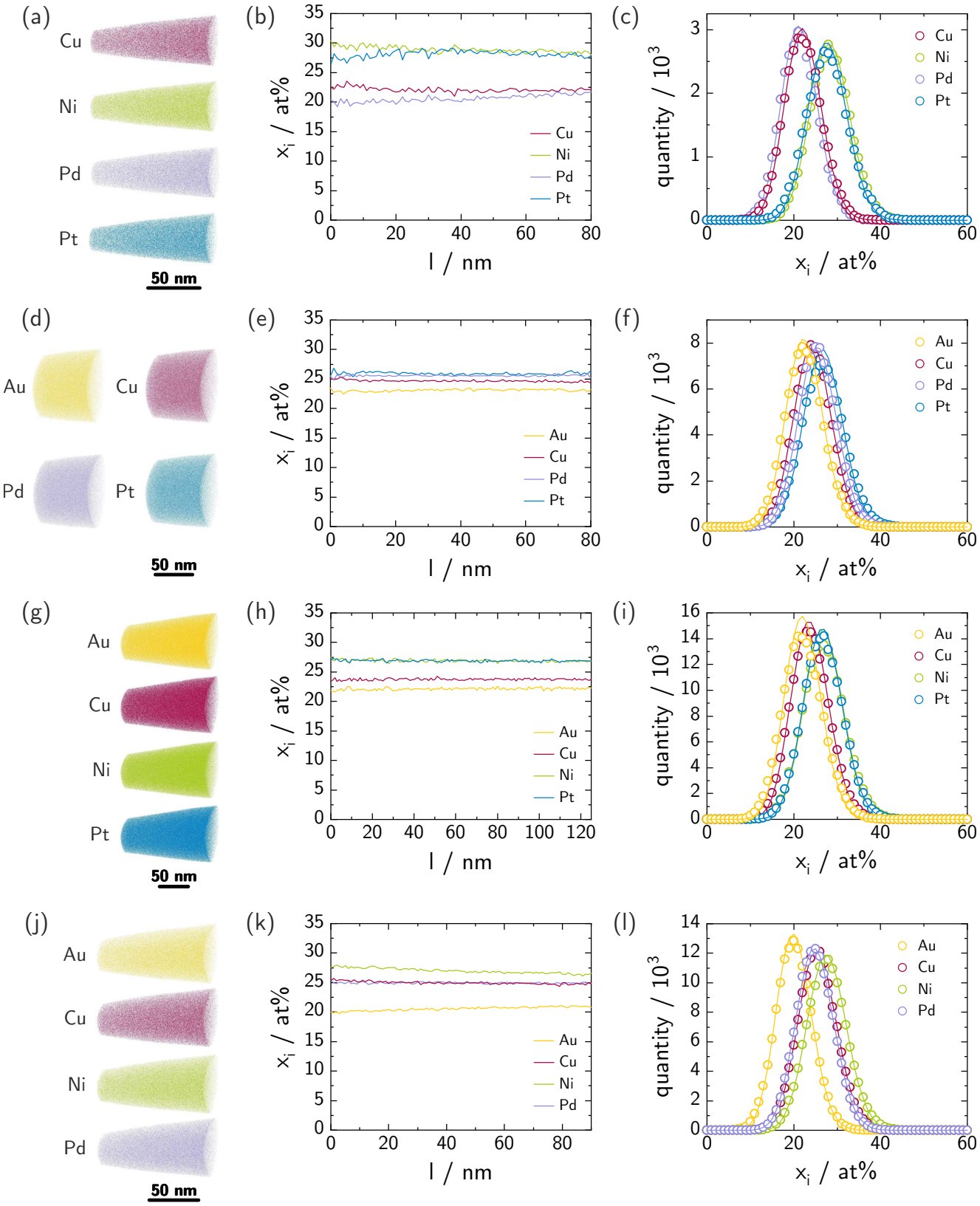

Figure 3: Atom probe tomography including the reconstruction of the sample tip with 10 % of detected ions, the concentration profile of components in longitudinal direction and the frequency distribution analysis of (a)–(c) CuNiPdPt, (d)–(f) AuCuPdPt, (g)–(i) AuCuNiPt and (j)–(l) AuCuNiPd.

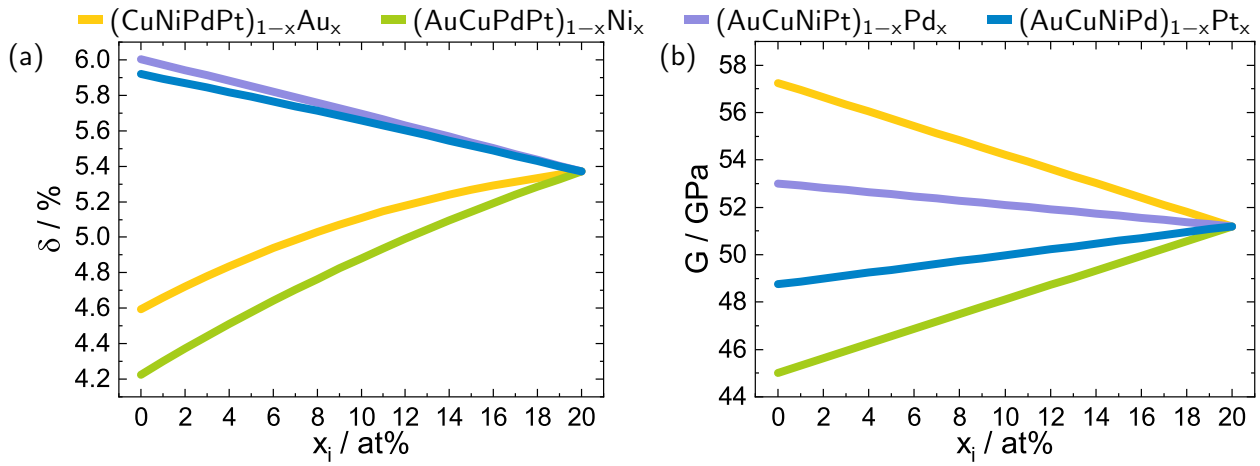

Figure 4: (a) misfit-parameter δ (calculated by Eq. 4) and (b) shear modulus G (calculated by Vegard's rule of mixture) depending on the chemical composition of solid solution series.

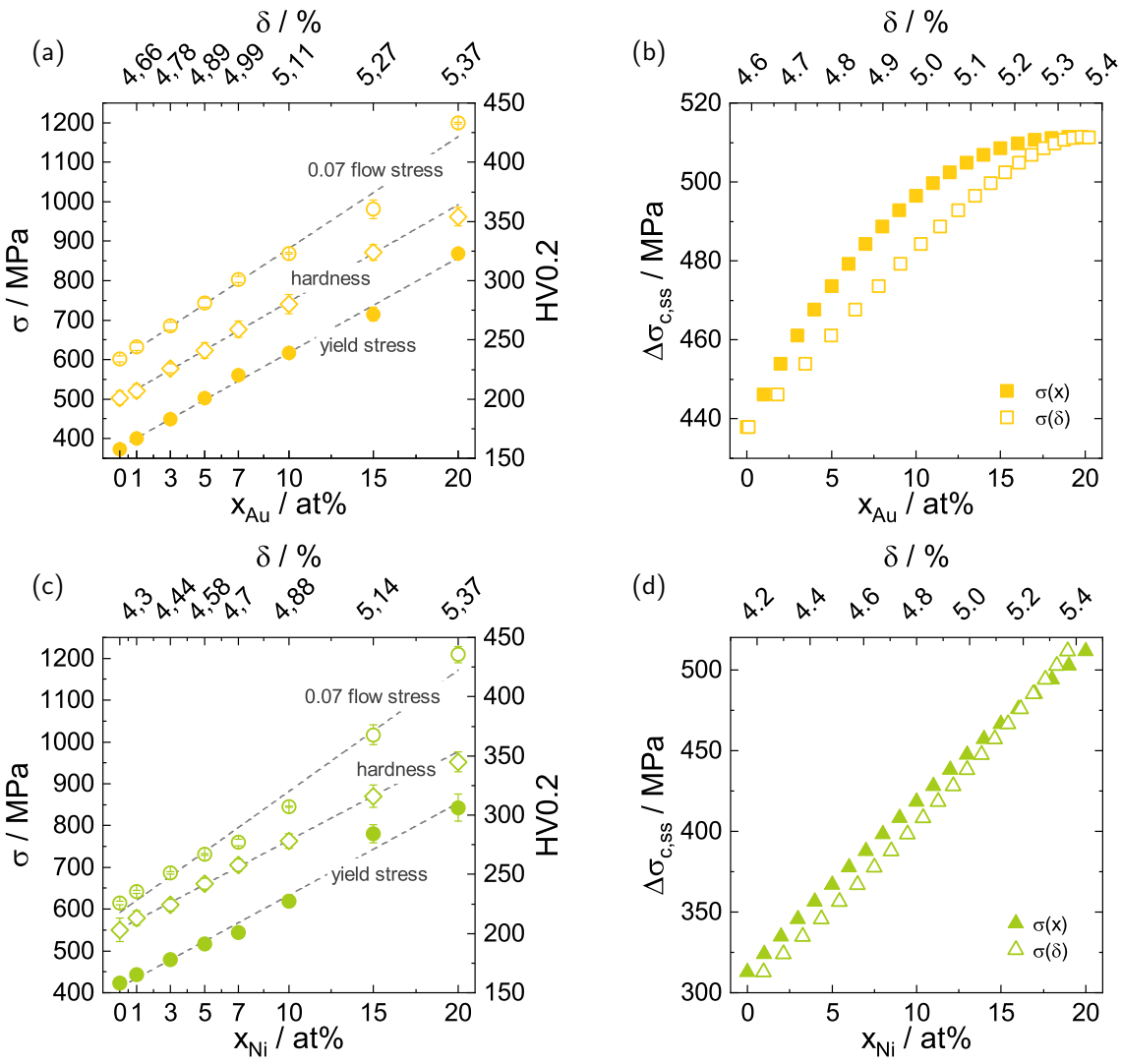

Figure 5: Mechanical properties in dependence of x_i and δ for (a) $(\mathrm{CuNiPdPt})_{100-x}\mathrm{Au}_x$ and (c) $(\mathrm{AuCuPdPt})_{100-x}\mathrm{Ni}_x$ as well as the corresponding calculations of the contribution of solid solution strengthening in (b) and (d) based on the Varvenne model. In case of (a) and (c) the x-axis are correlated.

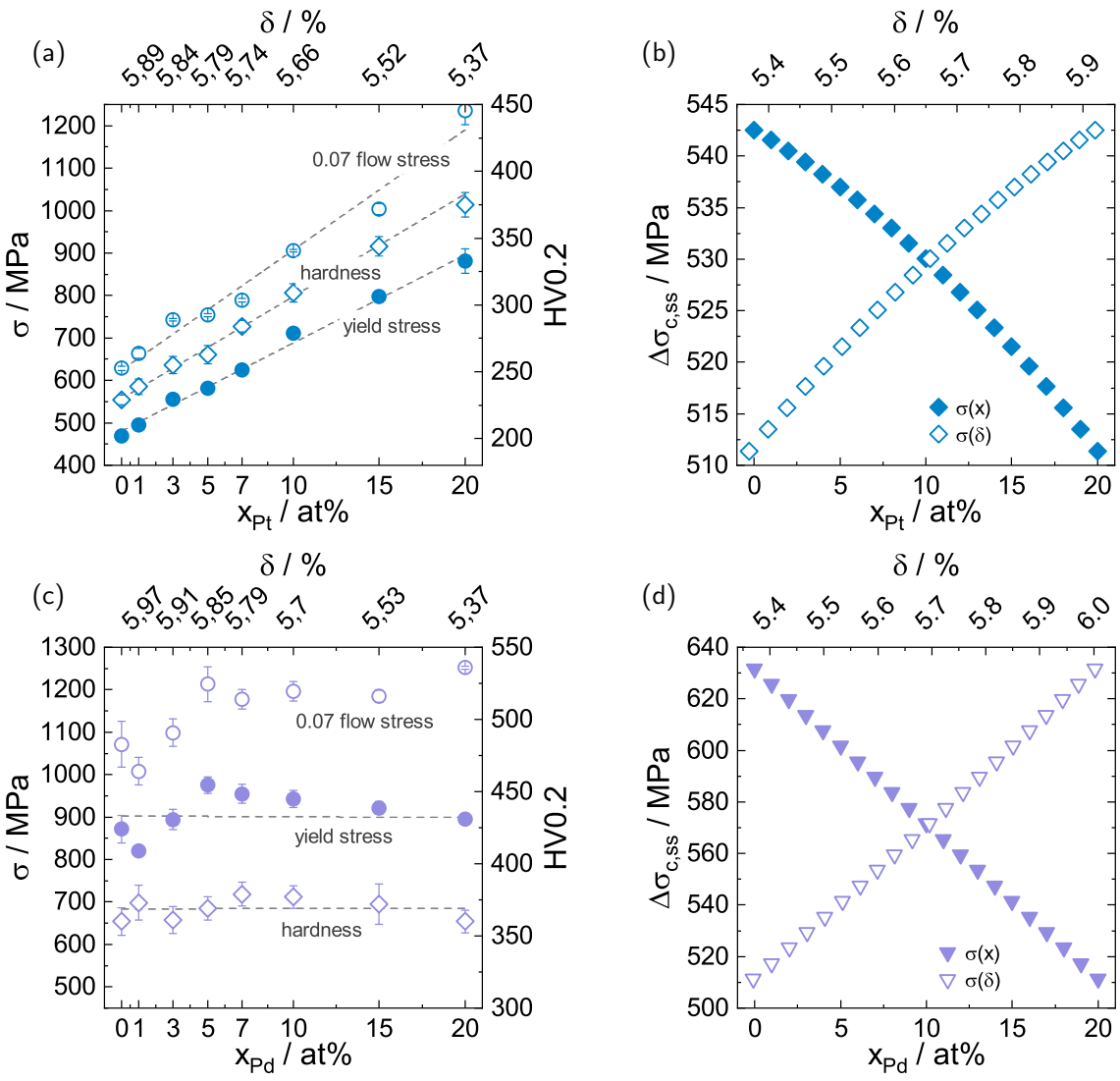

Figure 6: Mechanical properties in dependence of x_i and δ for (a) $(\mathrm{AuCuNiPt})_{100-x}\mathrm{Pd}_x$ and (c) $(\mathrm{AuCuNiPd})_{100-x}\mathrm{Pt}_x$ as well as the corresponding calculations of the contribution of solid solution strengthening in (b) and (d) based on the Varvenne model. In case of (a) and (c) the x-axis are correlated.